Computational and Structural Biotechnology Journal 19 (2021) 1620–1634

COMPUTATIONAL AND STRUCTURAL BIOTECHNOLOGY JOURNAL

journal homepage: www.elsevier.com/locate/csbj

A multiscale study on the mechanisms of spatial organization in ligand-receptor interactions on cell surfaces

Zhaoqian Su, Kalyani Dhusia, Yinghao Wu *

Department of Systems and Computational Biology, Albert Einstein College of Medicine, 1300 Morris Park Avenue, Bronx, NY 10461, United States

ARTICLE INFO

Article history:
Received 18 November 2020
Received in revised form 21 March 2021
Accepted 21 March 2021
Available online 23 March 2021

Keywords:
Ligand-receptor oligomerization
Multiscale simulation

ABSTRACT

The binding of cell surface receptors with extracellular ligands triggers distinctive signaling pathways, leading into the corresponding phenotypic variation of cells. It has been found that in many systems, these ligand-receptor complexes can further oligomerize into higher-order structures. This ligand-induced oligomerization of receptors on cell surfaces plays an important role in regulating the functions of cell signaling. The underlying mechanism, however, is not well understood. One typical example is proteins that belong to the tumor necrosis factor receptor (TNFR) superfamily. Using a generic multiscale simulation platform that spans from atomic to subcellular levels, we compared the detailed physical process of ligand-receptor oligomerization for two specific members in the TNFR superfamily: the complex formed between ligand TNFα and receptor TNFR1 versus the complex formed between ligand TNFβ and receptor TNFR2. Interestingly, although these two systems share high similarity on the tertiary and quaternary structural levels, our results indicate that their oligomers are formed with very different dynamic properties and spatial patterns. We demonstrated that the changes of receptor's conformational fluctuations due to the membrane confinements are closely related to such difference. Consistent to previous experiments, our simulations also showed that TNFR can preassemble into dimers prior to ligand binding, while the introduction of TNF ligands induced higher-order oligomerization due to a multivalent effect. This study, therefore, provides the molecular basis to TNFR oligomerization and reveals new insights to TNFR-mediated signal transduction. Moreover, our multiscale simulation framework serves as a prototype that paves the way to study higher-order assembly of cell surface receptors in many other bio-systems.

© 2021 The Authors. Published by Elsevier B.V. on behalf of Research Network of Computational and Structural Biotechnology. This is an open access article under the CC BY-NC-ND license (http://creativecommons.org/licenses/by-nc-nd/4.0/).

1. Introduction

Signaling pathways have been evolved in cells in order to adapt to their surrounding environments [1]. The first step of these pathways is to detect external stimuli to trigger the corresponding phenotypic variations of cells [2–5]. The detection of cellular stimuli is conducted by the dynamic interactions between cell surface receptors and extracellular ligands [6]. One typical example of extracellular ligands is called tumor necrosis factors (TNF), which is a major class of cytokines [7–9]. The binding of TNF with its target, TNF receptor (TNFR) on cell surface initiates multiple intracellular signaling pathways involved in inflammation [10–13]. Membrane receptors such as TNFR are anchored on cell surfaces. As a result, their ligand binding has very different properties from the interactions between proteins in solution. One major reason is that the movements of these membrane receptors are confined within cell surfaces. Intuitively, unlike freely diffusive soluble proteins which possess of three translational and three rotational degrees of freedom, cell surface receptor not only endure the loss of one translational degree of freedom, perpendicular to the membrane surface, but also experience the constraints on their rotational degrees of freedom [14,15]. Anchoring on the surface of plasma membrane, the conformational fluctuations of a receptor also highly depend on the flexibility of the linker region between its extracellular and transmembrane domains. These factors play important roles in mediating the kinetics of ligand-receptor interactions on cell surfaces. More importantly, it has been observed that a large variety of cell surface receptors, including TNFR superfamily, can aggregate into nanoscale oligomers upon ligand binding [16–20]. The organization of these supramolecular structures is a critical step towards the activation of intracellular signaling pathways [21]. The driven force beneath this cell-surface spatial organization, however, is multifaceted. Lipid raft [22] or

* Corresponding authors.
E-mail address: yinghao.wu@einstein.yu.edu (Y. Wu).

https://doi.org/10.1016/j.csbj.2021.03.024
2001-0370/© 2021 The Authors. Published by Elsevier B.V. on behalf of Research Network of Computational and Structural Biotechnology.
This is an open access article under the CC BY-NC-ND license (http://creativecommons.org/licenses/by-nc-nd/4.0/).

cytoskeletal activities [23] were believed to function in some systems, while in many other examples, such as cadherin and TNFR, a lateral binding interfaces between receptors exists, which is directly responsible to regulate their oligomerization [24]. Unfortunately, the molecular mechanism of how ligand-receptor interactions and additional interactions between receptors on the atomic level lead to their spatial organization on the subcellular level is not fully understood.

Traditionally, the *in vivo* binding between ligands and receptors on cell surfaces is relatively difficult to measure, and has only been successfully carried out in a limited number of cases [25]. Atomic force microscopy provides high spatial resolution to the dynamics of membrane proteins [26], but it is not suitable to study binding kinetics [27]. Fluorescence-based microscopy can be used to image membrane protein interactions on surfaces of individual cells [28–32]. However, it requires careful development of the appropriate labels for target proteins which may affect their activities in cells. On the other hand, binding constants of ligand-receptor interactions measured by *in vitro* experimental methods such as Isothermal Titration Calorimetry (ITC) [33] and surface plasma resonance (SPR) [34] isolate the interacting components from their usual biological surrounding, in order to permit a more convenient analysis that can't be done within the whole organisms. This leads to the large discrepancies between the *in vitro* and *in vivo* measuring systems [35,36]. In addition to the experimental studies, computational modeling possesses of unique advantages that permit one to test conditions that may currently be difficult to attain in the laboratory. Molecule-based techniques such as molecular dynamic (MD) [37–39] and Brownian dynamic (BD) [40–42] simulations have been used to study the dynamic properties of biomolecules. These approaches depend on the high-resolution structural information of individual molecules, and thus require extremely high computational resources. They are challenging to reach the timescale in which receptors form interactions with their ligands within the highly heterogeneous membrane environment. In contrast, a variety of low-resolution simulation approaches aimed to describe how collective behaviors of membrane receptors lead to spatial patterning on the subcellular level [43–52]. However, molecular details of receptors are rarely incorporated in these methods. As a result, multiscale modeling recently becomes a promising technique that can compensate the limitations within each computational model and bridge the dynamic information among different scales [53–55]. Some of these models combine atomic MD simulation with BD [56] or Monte-Carlo (MC) [57] simulations on a more coarse-grained (CG) level. In some other examples, CG force fields, such as MARTINI [58], were integrated into the multiscale models of MD simulations [59]. These methods have been applied to a large variety of biological systems over the last decade [60], including cell surface receptors on the plasma membrane [61]. Extension of these multiscale modeling approaches to understand the mechanisms of how ligand-receptor interactions form higher-order spatial organization on cell surfaces therefore is highly demanding.

In this article, a multiscale simulation framework was constructed to address these problems in ligand-binding induced receptor oligomerization. The complexes formed between ligands and receptors in TNF and TNFR superfamily is used as a test model (Fig. 1a). We compared the dynamics of receptor oligomerization between two specific systems: the complex formed between ligand TNFα and receptor TNFR1 versus the complex formed between ligand TNFβ and receptor TNFR2. The structural mode of ligand binding in these two systems is highly similar, but the regulation of their downstream signaling is very different [62]. TNFR1 is a type of death receptors (DR). Its cytoplasmic region contains a death domain (DD) [63]. On the other hand, there is no DD in the cytoplasmic region of TNFR2 and it activates intracellular signals

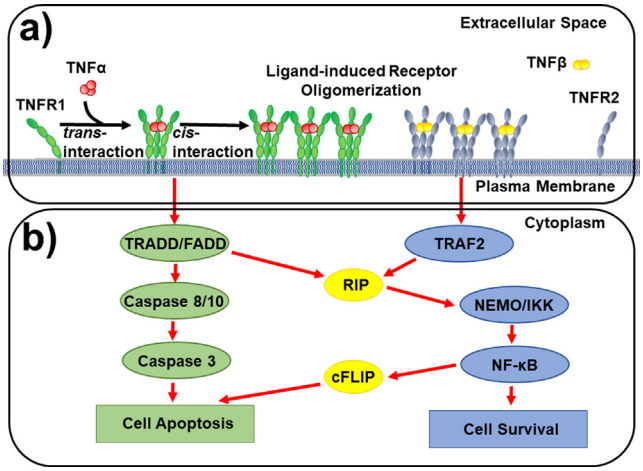

Fig. 1. More and more recent evidences show that spatial organization of ligand-receptor complexes on cell surface play a pivotal role in regulating cell signaling pathways. Here we use members in TNF and TNFR superfamily as a specific example. The cytokines TNFα and TNFβ form *trans*-interactions with cell surface receptors TNFR1 and TNFR2. These signaling complexes can further aggregate into oligomers through additional *cis*-interactions between receptors (a). In the cytoplasmic region, while activation of TNFR1 and TNFR2 modulates different pathways in immune responses, their signaling networks can also crosstalk with each other (b).

through interacting with different members in the TNF receptor associated factor (TRAF) family [64]. Both receptors share ligands TNFα and TNFβ and both TNFα and TNFβ ligands organize into homo-trimeric quaternary structures. Each subunit in the trimeric ligand adopts a β-sandwich "jelly-roll" fold [65]. On the other hand, the extracellular regions of both receptors TNFR1 and TNFR2 contain four tandem repeats of cysteine-rich domains (CRDs) [66]. Consequently, each trimeric ligand can simultaneously bind to three receptors, leading into the assembly of a ligand-receptor complex with a stoichiometry of 3:3. Within this complex, a TNFR1 or TNFR2 receptor binds at the interface between two consecutive subunits of its corresponding ligand. The structures of these ligand-receptor complexes are available between human TNFβ and TNFR1 at resolution 2.85 Å (PDB id 1TNR) [67] and between human TNFα and TNFR2 at resolution 3.00 Å (PDB id 3ALQ) [68]. Very recently, a structure of asymmetric complex between mouse TNFα and human TNFR1 has also been derived at resolution 3.15 Å (PDB id 7KP8) [20]. Finally, a dimeric structure was obtained between two TNFR1 at resolution 2.25 Å (PDB id 1NCF) [69].

Based on the structural information and our multiscale simulations, we found that the interactions in TNFβ-TNFR2 complex are in general weaker than TNFα-TNFR1 complex. In contrast, the confinement of plasma membrane introduces less restriction to TNFβ-TNFR2 complex. As a result, the difference of conformational flexibility between the monomeric and ligand-bound receptors in TNFα-TNFR1 system is larger than the difference in TNFβ-TNFR2 system. Interestingly, this relatively lower ratio of rigidity between the ligand-bound and monomeric receptors in TNFβ-TNFR2 complexes leads to the fact that the maximal size of oligomers formed by these complexes is statistically much larger than the oligomers formed by TNFα-TNFR1 complexes, although the binding in TNFβ-TNFR2 system is weaker. We speculate that the dynamic competition between monomeric receptors and ligand-receptor complexes due to the change of their conformational rigidity causes the difference of oligomerization in these two systems. Our results, therefore, provide new biological insights to the molecular basis of TNF-mediated receptor oligomerization and signal transduction. The framework of our multiscale simulation methods also serves as a prototype that paves the way to study higher-order assembly of cell surface receptors in many other signaling systems.

2. Results

2.1. A general description of the multiscale model on TNF ligand-receptor oligomerization

Experimental evidences suggest that the activation of TNFR1 and TNFR2 receptors not only triggers distinct signaling pathways, but their signaling networks can also crosstalk with each other (Fig. 1b) [70]. These findings imply that TNFR1 and TNFR2 may be selectively targeted for therapeutic purposes, offering opportunities to the context-specific treatment for autoimmune diseases [71]. Recent single-molecule imaging experiments further discovered that TNFα can induce the oligomeric state of functional TNFR1 clusters on plasma membrane of living cells [19]. The follow-up fundamental questions based on these experimental discoveries are: how differences in spatial patterns formed by other members of TNF and TNFR superfamily other than TNFα-TNFR1 oligomers can be captured; what are the molecular basis and functional implication of these differences. To tackle these problems, a multiscale computational framework was proposed to simulate the physical process of ligand-induced receptor oligomerization for TNFα-TNFR1 and TNFβ-TNFR2 complexes on their membrane surface.

The simulation of TNF ligand-induced receptor oligomerization is based on the diffusion–reaction algorithm with a domain-based coarse-grained model [72], as shown in the blue panel of Fig. 2. The bottom surface of the three-dimensional simulation box represents the plasma membrane, while the space above represents the extracellular region. TNFR receptors are distributed on the plasma membrane, while TNF ligands are placed in the extracellular region. Moreover, the molecular geometry was specifically designed to describe the structural arrangement of each TNF ligand and receptor. In detail, each subunit in a TNF ligand trimer is simplified by a rigid body with a radius of 3 nm [65], while these three rigid bodies are spatially organized into a three-fold symmetry in our model. On the other hand, four CRD domains in a receptor are coarse-grained into rigid bodies with radii of 2 nm, which are straightly aligned into rod-like shape [7]. The model consists of two types of interactions: the *trans*-interaction and the *cis* interaction. The "*trans*-interaction" is specifically defined by the interaction formed between a TNF receptor and one subunit in a trimeric TNF ligand. Since the ligands and receptors bind to each other through the *trans*-interactions, the trimeric ligand can simultaneously bind to three receptors and form a basic unit of signaling complex (Fig. 1a). The "*cis* interaction", on the other hand, is specifically defined by the interaction between two TNF receptors. The existence of a *cis* binding interface between two TNFR receptors is based on the evidence that a functionally conserved extracellular region across the TNFR superfamily was identified to modulate receptor assembly. This region is known as "pre-ligand assembly domain" (PLAD) and does not overlap with the *trans* binding interfaces [73,74]. As a result, the *cis* binding interface in a receptor is assigned on the opposite side of the *trans* binding interface, providing the possibility that ligand-receptor complexes are able to further aggregate into higher-order oligomers (Fig. 1a).

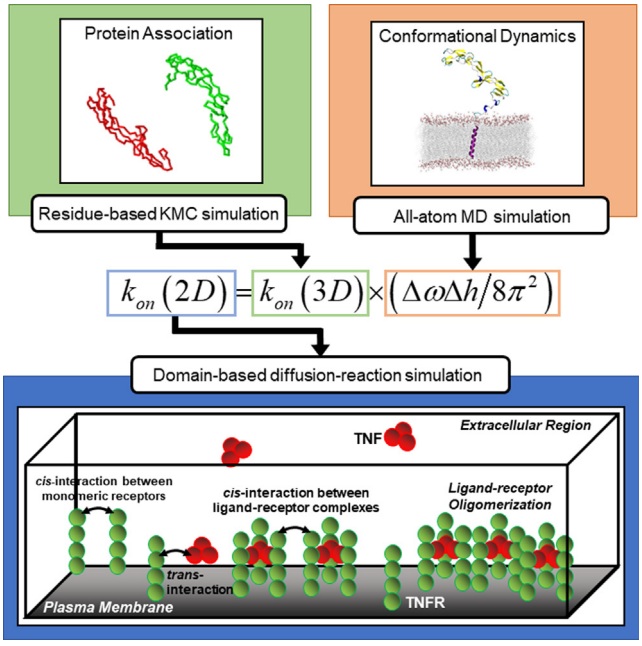

Fig. 2. The multiscale computational platform developed in this study integrates three simulation modules that spans from atomic to subcellular levels. The associations of all pairwise protein–protein interactions were simulated by a residue-based kinetic Monte-Carlo method, as shown in the green panel. In parallel, all-atom molecular dynamic simulations were applied to estimate conformational dynamics of receptors on plasma membrane, as shown in the red panel. Using the equation indicated in the middle of the figure, the impacts of membrane confinement on binding between receptors can be theoretically incorporated. Finally, these 2D binding rate constants were integrated into the domain-based diffusion reaction simulation (blue panel), so that the dynamics of receptor oligomerization on cell surfaces can be studied. (For interpretation of the references to colour in this figure legend, the reader is referred to the web version of this article.)

Given the model representation, an initial configuration can be generated by randomly distributing receptors on the plasma membrane and ligands in the extracellular region with predefined ligand concentration and receptor surface density. Starting from this initial configuration, the dynamics of the system is evolved by a standard diffusion reaction algorithm [75]. The detailed simulation procedure is described in the Methods. The binding rates in the simulations that are used to regulate the association and dissociation of the ligand-receptor *trans*-interactions and the *cis*-interactions between receptors are computationally estimated. Specifically, the protein–protein association rates are calculated by a residue-based kinetic Monte-Carlo (KMC) method developed in our previous study (green panel in Fig. 2) [76]. The KMC simulations are conducted in three-dimensional (3D) environments. However, the receptors involved in a *cis*-interaction are anchored on the surface of plasma membrane, which is a two-dimensional (2D) environment. In order to taken the effect of membrane confinement on *cis*-interactions into account, full-length structural models of receptors, as well as ligand-receptor complexes were built and embedded into lipid bilayers. All-atom molecular dynamic simulations were further applied to extract the information about conformational dynamics in these systems (red panel in Fig. 2). Using the equation indicated in the figure, as we originally derived based on the statistical thermodynamics, the 3D binding constants calculated from KMC simulations can be theoretically transferred into 2D. Finally, these 2D binding rate constants are integrated into the domain-based coarse-grained mode, so that we can compare the spatial patterns and dynamics of TNFα-TNFR1 and TNFβ-TNFR2 oligomerization on cell surfaces with atomic details.

2.2. Calculate the association rates for binding involved in ligand-receptor oligomerization

The oligomerization of TNF ligand-receptor complexes requires both *trans*-interactions between TNF ligands and TNFR receptors, as well as the *cis*-interactions between TNFR receptors. We used our previously developed residue-based kinetic Monte-Carlo simulation method to estimate the association rates for these two types of interactions. The detailed algorithm of the simulation is

described in the Methods. In practice, *trans* and *cis* interactions were simulated separately. The association of *trans*-interactions between TNFα and TNFR1 was first tested and compared with the *trans*-interactions between TNFβ and TNFR2. Since of the experimental structures are not available for both *trans*-interactions, computational models were used to assess the conformation of encounter complexes formed in the simulations. Specifically, the *trans*-binding interface between a trimeric TNFα ligand and a monomeric TNFR1 receptor was adopted from a previous model built by Chen and coworkers [77]. Similarly, the atomic coordinates of *trans*-interaction between a trimeric TNFβ ligand and a monomeric TNFR2 receptor was modeled by using the crystal structure of TNFα-TNFR2 complex (PDB id 3ALQ) as a template.

After the model construction of the final complex in both systems, ligands and receptors were coarse-grained with a residue-based representation described in the Methods. They were then separated from each other and randomly placed in the 3D space such that the distance between their binding interfaces is constrained within a cutoff value d_c, as shown in Fig. 3a. Following the initial conformations, both molecules move towards each other with the presence of a simplified force-field to describe the intermolecular interaction. For each specific value of distance cutoff, 10^3 simulation trajectories were generated from different initial conformations. By comparing the conformations of ligands and receptors in the simulations with the model of final complex, we found that they diffused away and failed to find each other in some trajectories, but successfully form encounter complexes in others. We further changed the distance cutoff from 15 Å to 20 Å, and calculated the association probability by counting how frequently encounter complexes were formed among all trajectories under each cutoff value.

The relations between the distance cutoff d_c and the association probability are plotted for both TNFα-TNFR1 (black circles) and TNFβ-TNFR2 (red circles) systems in Fig. 3b. The figure shows that the highest association probabilities in both systems are obtained when the value of distance cutoff equals 15 Å. However, the association probabilities then drop as the distance cutoff increases, indicating that the TNF-TNFR complexes are more difficult to form if they are initially separated farther from each other. Moreover, comparing the association probabilities of interactions between TNFα and TNFR1 with the interactions between TNFβ-TNFR2, we found that the former is much higher than the latter. This result suggests that the formation of TNFα-TNFR1 complex is much faster than TNFβ-TNFR2 complex. Finally, the profiles of association probability in both systems were used to derive the association rates of *trans*-interactions. As a result, the rate of TNFα-TNFR1 association equals 0.025 ns^{-1}; while the rate of TNFβ-TNFR2 association is about five-fold lower (0.0055 ns^{-1}). These parameters later will be used in the domain-based simulations.

In parallel to the *trans*-interaction, the association of *cis*-interactions formed between two TNFR1 or TNFR2 receptors was evaluated by the same residue-based kinetic Monte-Carlo simulation approach (Fig. 3c). Two TNFR1 receptors were observed to form a lateral dimer in a recent x-ray crystal structure [69], which is thought to be in the *cis* configuration. The atomic coordinates of a TNFR1-TNFR1 *cis*-dimer therefore were taken from this experimental structure (PDB id 1ncf). Based on the experimental evidences that the PLAD region is functionally conserved across various members in TNFR superfamily, as well as the high structural similarity between TNFR1 and TNFR2, we assume that TNFR2 receptors can form *cis*-interactions through the same interface. As a result, the PDB structure 1ncf was used as a template to build the model of TNFR2-TNFR2 *cis*-dimer using rigid-body structural alignment. Following the same simulation procedure, we changed the distance cutoff from 15 Å to 20 Å. For each specific value of distance cutoff, 10^3 simulation trajectories were carried out and the association probabilities were calculated. The relations between the distance cutoff and the association probability are plotted for

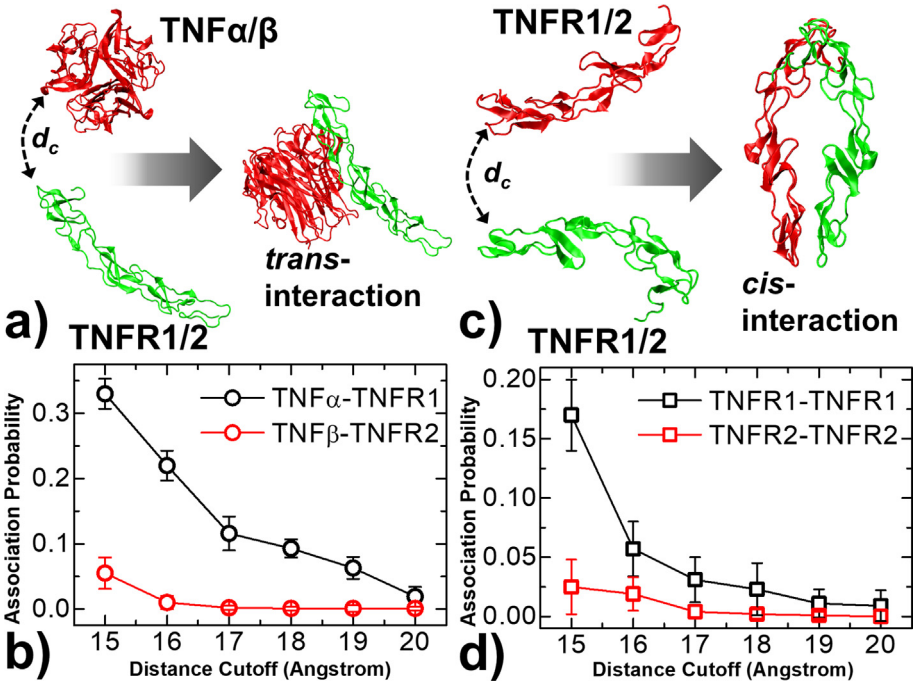

Fig. 3. We simulated the association between TNF and TNFR by a residue-based kinetic Monte-Carlo algorithm (a). Multiple simulation trajectories were started from different values of distance cutoff d_c. We counted the association probability by counting of how many encounter complexes were formed among these trajectories. We compared the probabilities of association between TNFα and TNFR1 (black) with the association between TNFβ and TNFR2 (red) under different distance cutoff values. They are plotted in (b) with error bars. We further simulated the association of *cis*-interactions between two TNFR receptors (c). The association probabilities between two TNFR1 (black) under different values of distance cutoff were compared with the probabilities between two TNFR2 (red). They are shown in (d) with error bars. (For interpretation of the references to colour in this figure legend, the reader is referred to the web version of this article.)

both TNFR1-TNFR1 (black circles) and TNFR2-TNFR2 (red circles) systems in Fig. 3d. The figure indicates that *cis*-interactions in general have lower association probability than the *trans*-interaction, while the association of TNFR1-TNFR1 dimer is much faster than TNFR2-TNFR2 dimer. The association rates were finally derived from the distributions for TNFR1-TNFR1 *cis*-interaction (0.017 ns^{-1}) and TNFR2-TNFR2 *cis*-interaction (0.0025 ns^{-1}).

2.3. Estimate the effect of membrane confinement on cis-interactions between receptors

It has been found that members in TNFR superfamily, including TNFR1 and TNFR2, are able to preassemble into lateral dimers on cell surfaces through their functionally conserved PLAD regions. The formation of this *cis*-interaction between TNFR monomers is independent of ligand binding. Its association rate has been estimated by our residue-based kinetic Monte-Carlo simulations, in which two receptors can freely diffuse in 3D space. However, these receptors are anchored on plasma membrane in real cellular environments. This 2D membrane confinement can cause unneglectable impacts on kinetic properties of binding between receptors. Moreover, experimental evidences showed that ligand-binding induces higher-order oligomerization, indicating that the *cis*-interactions between receptors can be regulated by the formation of signaling complexes through the ligand-receptor *trans*-binding interfaces and thus trigger their lateral assembly. The molecular mechanism of the interference between the *trans*- and *cis*-interactions, unfortunately, is not well understood. We hypothesize that the conformational fluctuations of TNFR receptors in their monomeric and ligand-bound states are different. Intuitively, all three receptors in a signaling complex are tethered to plasma membrane and thus there are more constraints in dynamics of the complex than monomers. The difference in the configurational entropy between monomeric and ligand-bound states of receptors can further affect the rate of their association. As a result, we assume that the 2D association rates of a *cis*-interaction between two monomeric receptors should be different from the interaction between receptors in their ligand-bound states.

Fortunately, the effects of membrane confinements and conformational fluctuations on molecular binding can be theoretically estimated. Based on the theory of statistical thermodynamics [78], and assuming that membrane confinements only affect the process of association between two proteins but not their dissociation, the relation between the rate $k_{on}^{cis}(3D)$ in which two receptors form a *cis*-interaction in solution and the rate $k_{on}^{cis}(2D)$ in which they form a *cis*-interaction on plasma membrane has the following form.

$$\frac{k_{on}^{cis}(3D)}{k_{on}^{cis}(2D)} = \frac{1}{8\pi^2} \times \Delta\omega\Delta h \quad (1)$$

In Eq. (1), Δh represents the range of conformational fluctuations in membrane-bound receptors along membrane normal, while $\Delta\omega$ corresponds to the volume in the rotational phase space of membrane-bound receptors. The value of 3D association rate $k_{on}^{cis}(3D)$ for the *cis*-interactions was estimated in the last section. Moreover, the difference between the rate $k_{on}^{cis}(2D,M)$ in which a *cis*-interaction is formed by two monomeric surface-bound receptors and the rate $k_{on}^{cis}(2D,C)$ in which the same *cis*-interaction is formed by ligand-bound receptors, or ligand-receptor signaling complexes on cell surfaces, can be written as follow.

$$\frac{k_{on}^{cis}(2D,C)}{k_{on}^{cis}(2D,M)} = \frac{\Delta\omega_M\Delta h_M}{\Delta\omega_C\Delta h_C} \quad (2)$$

In Eq. (2), Δh_M and Δh_C represent the range of conformational fluctuations along membrane normal for membrane-bound receptors in their monomeric (M) or ligand-bound complex (C) states, respectively. Similarly, $\Delta\omega_M$ and $\Delta\omega_C$ correspond to the volume in the rotational phase space of membrane-bound receptors in their monomeric or ligand-bound complex states. Detailed procedure of deriving Eqs. (1) and (2) can be found in the Supporting Information.

Practically, the distributions of conformational parameters Δh and $\Delta\omega$ in both Eqs. (1) and (2) were derive from all atom molecular dynamic simulations. In detail, the conformational fluctuations in four systems were specifically considered: 1) the system contains a single TNFR1 receptor on lipid bilayer (Fig. 4a); 2) the system contains a single TNFR2 receptor on lipid bilayer (Fig. 4b); 3) the system contains a TNFα-TNFR1 signaling complex on lipid bilayer (Fig. 4c); and 4) the system contains a TNFβ-TNFR2 signaling complex on lipid bilayer (Fig. 4d). Details about the model constructions and simulation protocols are described in the Methods.

The distributions of receptor's conformational fluctuations along membrane normal are plotted in Fig. 4e for the above four systems, while the ranges of Δh are defined as twice the standard deviation of these distributions. The figure shows that the ranges of distributions in two TNFR2 involved systems (the lower two panels of Fig. 4e) are wider than the corresponding TNFR1 involved systems (the upper two panels of Fig. 4e). For instance, the calculated value of Δh_M for TNFR1 monomer equals 24 Å, while the value for TNFR2 monomer equals 47 Å. For ligand-receptor complex, the values of Δh_C for TNFα-TNFR1 and TNFβ-TNFR2 complexes equal 13 Å and 20 Å, respectively. This suggests that the structural flexibility of TNFR2 on membrane surfaces is higher than TNFR1. Moreover, comparing the conformational fluctuations in monomeric receptors (the left two panels of Fig. 4e) with the fluctuations in ligand-bound receptors (the right two panels of Fig. 4e), we found that the fluctuations of monomers are much wider than their corresponding complexes, confirming our assumption that ligand-binding adds more restrictions to the dynamics of receptors.

In addition to the range of translational fluctuations, we also measured the conformational dynamics in the rotational phase space, which can further be characterized by three Euler angles as $\Delta\omega = \Delta\psi \times \Delta\varphi(1 - \cos\Delta\theta)$ [78]. As shown in Fig. 5a and 5b, φ is defined as the angle around the membrane normal z, ψ is defined as the angle around the long principal axis z′ of the protein, and θ is the tilting angle between this principal axis and the membrane normal. The detailed distributions of these angles in the four testing systems are shown in Fig. 5c-5f, while the ranges of these distributions are defined as twice of their standard deviations and can be found in the supporting information as Table S2. Similar to the translational fluctuations, the angular fluctuations in monomers (Fig. 5c and 5e) are much wider than in the corresponding complexes (Fig. 5d and 5f). Finally, when we integrated the ranges of all conformational parameters into equation (2), we found that the ratio between $k_{on}^{cis}(2D,C)$ and $k_{on}^{cis}(2D,M)$ in TNFR1 equals 20, much larger than the ratio of TNFR2 (11). Both ratios are one order of magnitude larger than 1, indicating that the association rates of *cis*-interactions between ligand-bound receptors in both systems are significantly enhanced. We suggest that this is due to the loss of configurational entropy in the TNFR receptors after their ligand binding. Moreover, the higher ratios in TNFR1 indicate that its *cis*-interaction after ligand binding is more affected than TNFR2. This difference leads to the result that TNFR1 and TNFR2 attain distinguishable patterns during their oligomerization, as we will show in the next section.

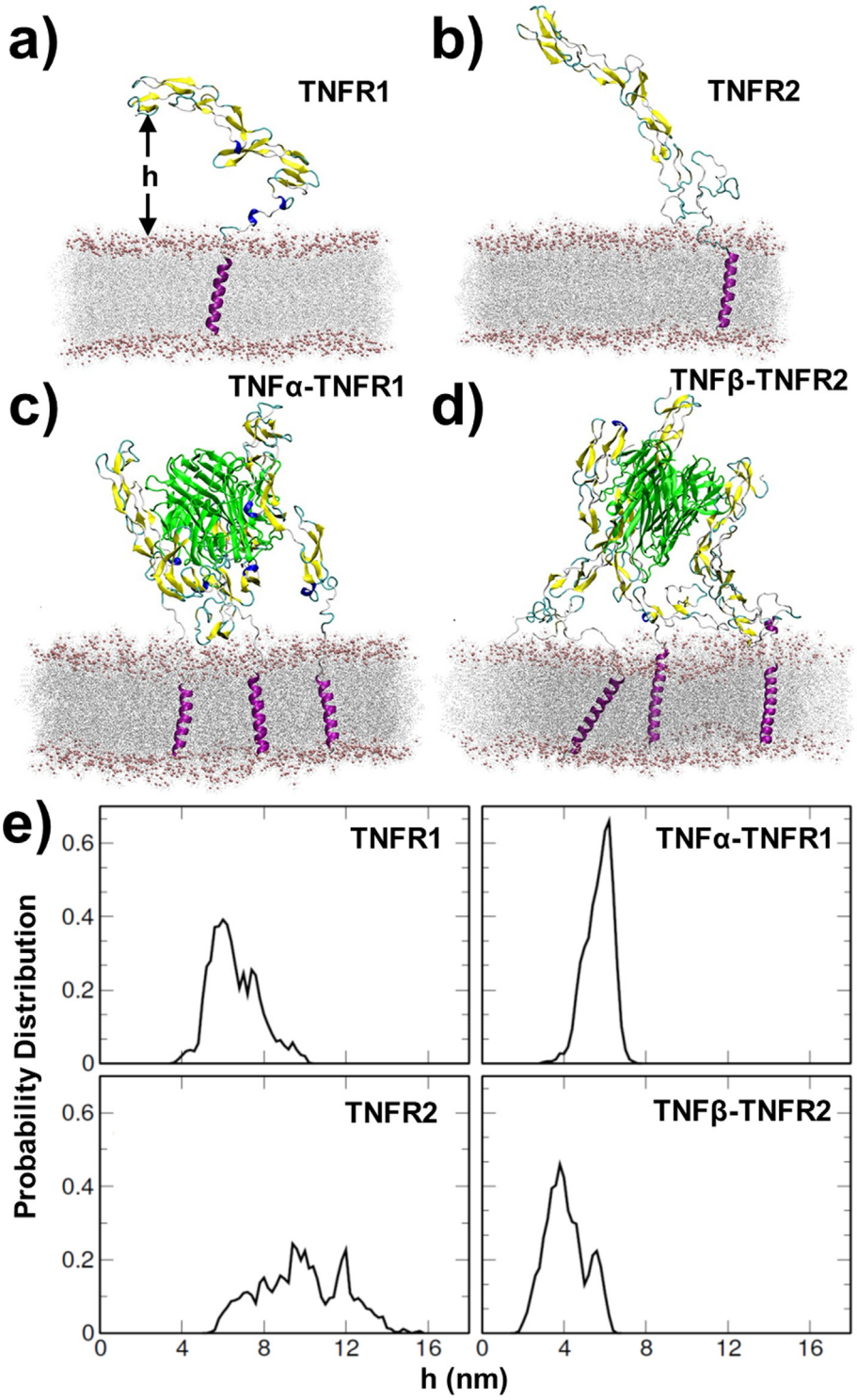

Fig. 4. In order to evaluate the differences in conformational fluctuations between monomeric and ligand-bound TNFR receptors, four structural models were constructed as inputs for all-atom molecular dynamic simulations. Specifically, these are the system contains a single TNFR1 receptor on lipid bilayer (a); the system contains a single TNFR2 receptor on lipid bilayer (b); the system contains a TNFα-TNFR1 signaling complex on lipid bilayer (c); and the system contains a TNFβ-TNFR2 signaling complex on lipid bilayer (d). Based on the molecular dynamic simulation result, the distributions of receptor's conformational fluctuations along membrane normal, h, were derived for the above four systems, as shown in (e).

2.4. Observe the difference in spatial patterns of oligomerization between TNFR1 and TNFR2

In order to study ligand-receptor oligomerization, binding parameters, including the association and dissociation rates of the ligand-receptor *trans*-interactions and the *cis*-interactions between receptors, were incorporated into our domain-based diffusion–reaction simulations. Binding constants of *trans*-interactions between members in TNF and TNFR superfamily have been measured by various experimental methods such as

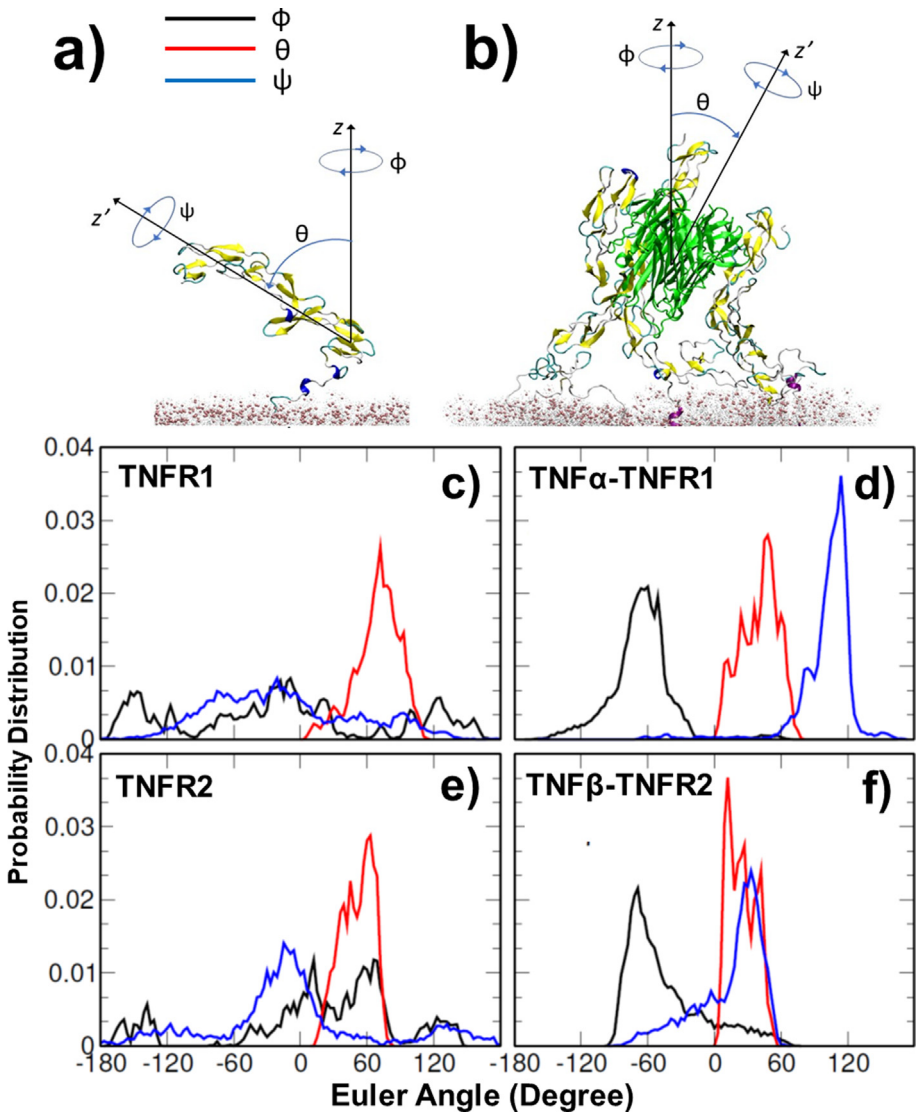

Fig. 5. The conformational dynamics in the rotational phase space can be characterized by three Euler angles, as illustrated in (a) for monomeric receptor and (b) for ligand-receptor complex. The detailed distributions of these angles from molecular dynamic simulations are shown in (c) for the system containing a single TNFR1 receptor; in (d) for the system containing a TNFα-TNFR1 signaling complex; in (e) for the system containing a single TNFR2 receptor; in (f) for the system containing a TNFβ-TNFR2 signaling complex.

homogenous time resolved fluorescence (HRTF) and surface plasma resonance (SPR) [79]. Unfortunately, these measurements often varied over several orders of magnitude due to different experimental conditions. Moreover, the binding rates of *cis*-interactions among receptors have never been previously characterized. As a result, the association rates of both *trans* and *cis* interactions were computationally calculated by our residue-based kinetic Monte-Carlo simulations. The association rates of *cis*-interactions have further been transformed from 3D to 2D form based on theoretical analysis and the statistical distributions from all-atom molecular dynamic simulations. In order to obtain the value of dissociation ratesk_{off}, we plugged the calculated associate rates along with binding affinity ΔG into the equation$k_{off} = k_{on} \times \exp(\Delta G/RT)$, in which the values of binding affinity for *trans*-interactions in TNFα-TNFR1 and TNFβ-TNFR2 complexes, as well as for *cis*-interactions of TNFR1-TNFR1 and TNFR2-TNFR2 dimer, were calculated by the program DCOMPLEX. DCOMPLEX provides an accurate prediction to binding affinity of protein complexes using the structure-derived statistical potential [80]. All detailed values of these calculated binding rates and affinities can be found in Table S3 for both TNFR1 and TNFR2 systems.

In addition to the binding rates, values of other parameters in the domain-based simulations are specified as follow. The lengths of each side along both X and Y directions of the simulation box are 1000 nm, which gives the surface of plasma membrane a total area of 1 μm^2. Along the Z direction, the height of the simulation box is 100 nm. The number of trimeric TNF ligands was fixed at 150 and the number of TNFR1 or TNFR2 receptors was fixed at 450. Consequently, the surface density of receptors is on the order of ~$10^2 mol/\mu m^2$. This surface density is within the typical range that was experimentally observed in T cells [81]. The soluble ligands TNFα and TNFβ undergo three-dimensional diffusions freely in the extracellular region. The translational diffusion coefficients for both TNFα and TNFβ are 72.6 $\mu m^2/s$ and their rotational coefficients is $0.34°ns^{-1}$, calculated by a precise boundary element method [82]. Relatively, due to the restriction of plasma membrane, the two-dimensional diffusions of a TNFR1 or TNFR2 receptor are much slower, with a translational constant of 10 $\mu m^2/s$ and rotational coefficient of $1°ns^{-1}$. These values were

adopted from our previous all-atom molecular dynamic simulations [83]. Moreover, diffusions of a signaling complex on membrane surface are considered as even slower, with a translational constant of 5 $\mu m^2/s$ and rotational coefficient of $0.28°ns^{-1}$. Finally, in order to attain statistically meaningful result, multiple simulation trajectories were carried out. In specific, 13 replicas were generated for TNFα-TNFR1 system and 16 replicas were generated for TNFβ-TNFR2 system. Each trajectory was started from a randomly generated initial configuration, as shown in Fig. 6a. All trajectories were terminated when their time length reached 6×10^8ns, while the length of each simulation step is 10 ns.

We compare the kinetic profiles of patterns formed in the TNFα-TNFR1 system with the TNFβ-TNFR2 system. These profiles were averaged over all the simulation trajectories. The numbers of *trans*-interactions were first plotted in Fig. 6b as a function of simulation time. The interactions formed between TNFα ligands and TNFR1 receptors are shown in the black curve, while the interactions formed between TNFβ ligands and TNFR2 receptors are shown in the red curve. The figure shows that more *trans*-interactions were formed in the TNFα-TNFR1 system than the TNFβ-TNFR2 system, which is consistent with the previous experimental information. Moreover, the TNFα-TNFR1 system reached equilibrium before 1×10^8ns, while the TNFβ-TNFR2 system reached equilibrium after 1×10^8ns. This is based on the result that the association rate of *trans*-interaction between TNFα and TNFR1 is higher than between TNFβ and TNFR2. In comparison, the numbers of *cis*-interactions between ligand-bound and monomeric receptors were further plotted in Fig. 6c and 6d, respectively. Fig. 6c shows that more *cis*-interactions between ligand-bound TNFR1 receptors were formed than between ligand-bound TNFR2 receptors. In contrast, as the numbers of ligand-bound *cis*-interaction increased and then reached equilibrium, Fig. 6d shows that the number of monomeric *cis*-interaction reached maximal level at the very early stage of the simulations and then dropped. Different from the TNFR1 system in which almost no monomeric *cis*-interaction left, the monomeric *cis*-interaction in the TNFR2 system remained at a low level throughout the simulation.

In order to quantify the spatial characteristics of ligand-receptor oligomers formed in both systems, the average size of clusters observed along simulations were plotted in Fig. 6e. This average size of oligomers is directly comparable to a recent single-molecule image experiment [19]. In the meanwhile, a final snapshot was taken from one representative trajectory of each system to further visualize the spatial distribution of these clusters.

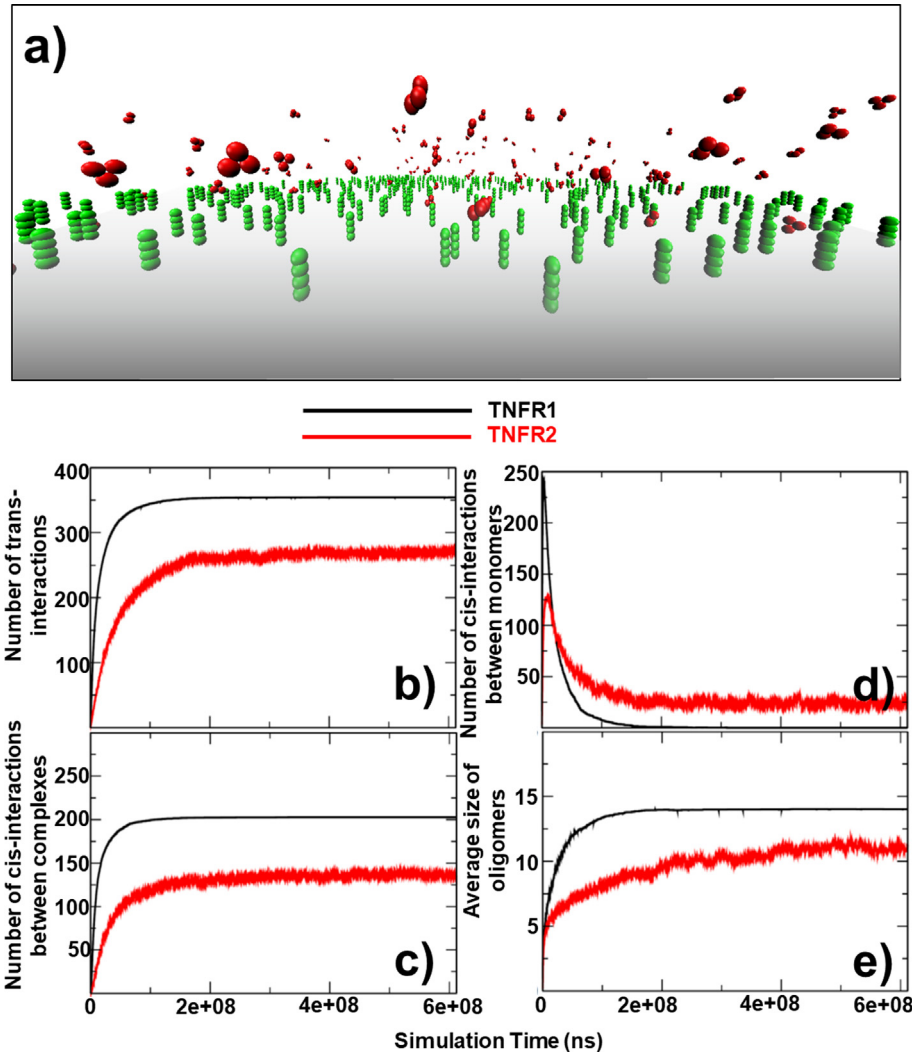

Fig. 6. All parameters estimated from residue-based and all-atom simulations were incorporated into our domain-based diffusion–reaction simulations. Multiple simulation trajectories were carried out and each one was started from a randomly generated initial configuration, as shown in (a). We compare the kinetic profiles averaged from the TNFα-TNFR1 system with the TNFβ-TNFR2 system as a function of simulation time. These profiles include the numbers of *trans*-interactions (b); the numbers of ligand-bound *cis*-interactions (c); the numbers of monomeric *cis*-interactions (d); and the average sizes of oligomers formed in the simulations (e).

The top-view from the final configuration of the TNFα-TNFR1 system is shown in Fig. 7a, while Fig. 7b is the TNFβ-TNFR2 system. In both figures, ligand-receptor complexes are organized into hexagonal lattice. The same spatial pattern of ligand-induced clustering was also proposed for TNFα-TNFR1 system based on recent experimental studies. Specifically, precipitation was observed in a recent *in vitro* experiment by spectrophotometry and gel densitometry, when TNFα and TNFR1 were mixed [20]. The author suggested that these aggregates are an ordered protein network stabilized by specific TNFα–TNFR1 and TNFR1–TNFR1 interactions. Moreover, in another recent study, clustering of TNFR1 upon binding of TNFα was directly detected by quantitative, single-molecule super-resolution microscopy at physiological cell surface abundance and in native cellular settings [19]. The authors highlighted the importance of *cis* dimerization between TNFR1 in the assembly of higher-order oligomers. Unfortunately, the experimental measurement of oligomerization in TNFβ-TNFR2 system has not been documented.

Surprisingly, although Fig. 6e suggests that average size of TNFα-TNFR1 oligomers is slightly larger than TNFβ-TNFR2 oligomers, we found that some oligomers formed by TNFβ-TNFR2 signaling complexes (Fig. 7b) are much larger than the oligomers formed by TNFα-TNFR1 signaling complexes. This is further confirmed by Fig. 7c, in which the sizes of the largest oligomer

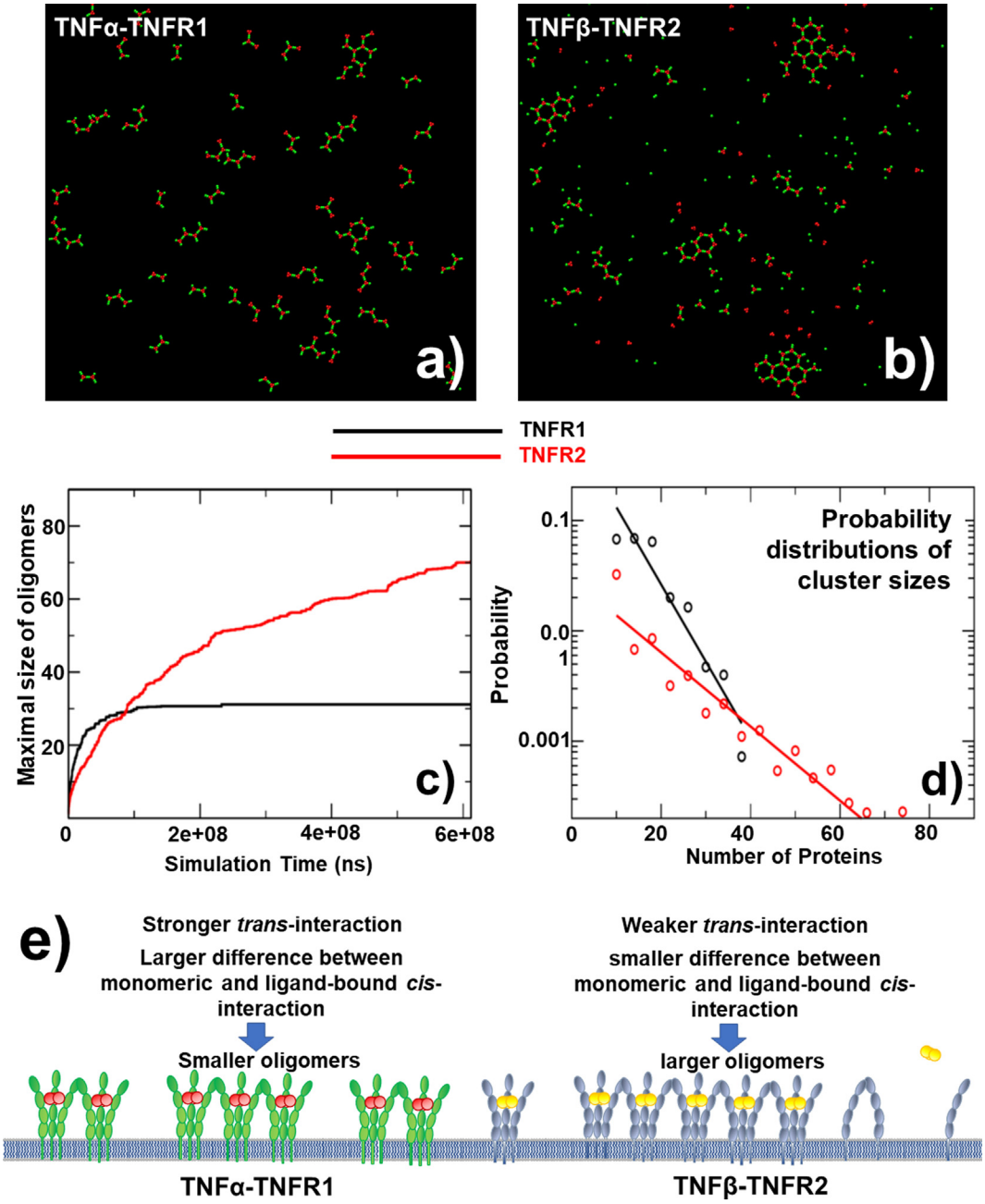

Fig. 7. Final snapshots were taken from one representative trajectory of TNFα-TNFR1 (a) and TNFβ-TNFR2 (b) systems to further visualize the spatial configuration of these oligomers. We further compared the maximal (c) and probability distribution (d) of oligomer sizes between TNFR1 (black) and TNFR2 (red) systems. Our simulation results are summarized in (e). In brief, we suggest that the oligomers formed by TNFα-TNFR1 complexes can be stabilized very fast (left-hand side). In contrast, the oligomerization of TNFβ-TNFR2 complexes is much slower but dynamic, while the largest TNFβ-TNFR2 oligomers almost double the size of the largest TNFα-TNFR1 oligomers (right-hand side). (For interpretation of the references to colour in this figure legend, the reader is referred to the web version of this article.)

observed from all trajectories of two systems are compared with each other. The figure also shows the difference in the dynamics of their oligomerization. While the large oligomers formed by TNFα-TNFR1 signaling complexes were stabilized very fast (black curve in Fig. 7c), the growth of oligomers formed by TNFβ-TNFR2 signaling complexes was relatively much slower. This growth was not stopped until the end of the simulation (red curve in Fig. 7c). As a result, the largest TNFβ-TNFR2 oligomers more than doubled the size of the largest TNFα-TNFR1 oligomers. Finally, the probability distributions of all cluster sizes in two systems are compared, as shown in Fig. 7d. Given the logarithmic scale of the y-axis, the figure indicates that the cluster size distributions in both systems can be fitted by a single exponential function. The size distribution functions also verify that TNFα-TNFR1 signaling complexes tend to have higher probability to form oligomers with smaller sizes, while TNFβ-TNFR2 oligomers have the feasibility to grow into very large clusters. Our computationally predicted features in cluster size distributions and the differences between TNFR1 and TNFR2 systems can be directly validated by experiments such as single-molecular tracking or super-resolution imaging.

Our simulation results suggest that TNFα-TNFR1 signaling complexes prefer forming oligomers with smaller average size and standard deviation. We speculate that the differences in the binding rates of *trans*-interactions between TNFα-TNFR1 and TNFβ-TNFR2 systems, and more importantly, their ratios of conformational fluctuations between the monomeric and ligand-bound receptors play important roles. Specifically, the TNFα-TNFR1 system has stronger binding affinity and higher association rate of *trans*-interaction. Meanwhile, its higher ratio of conformational fluctuations embedded in Eq. (2) leads into the result that the *cis*-interaction between ligand-bound TNFR1 receptors is much more strengthen, comparing with the *cis*-interaction between monomeric receptors. As a result, TNFα and TNFR1 can form complexes more easily, while these complexes are more difficult to dissociate and thus kinetically trapped in small oligomer due to the strong *cis*-interactions between ligand-bound receptors, as shown on the left-hand side of Fig. 7e. Unlike TNFα-TNFR1 system, the oligomers formed by TNFβ-TNFR2 signaling complexes are more dynamic. Relatively weaker binding and slower association of its *trans*-interaction result in a number of unbound receptors in the system. Meanwhile, the *cis*-interaction between ligand-bound TNFR2 receptors is less strengthen, reflected by its relatively lower ratio of conformational fluctuations embedded in equation (2). This leads to the result that an equilibrium state between oligomers formed by ligand-bound receptors and lateral dimers formed by monomeric receptors remains throughout the simulation, as indicated by Fig. 6d. This dynamic equilibrium ensures that the oligomers are constantly reorganized. As a result, small oligomers have higher probabilities to dissolve or merge into oligomers with larger size, as shown in the right-hand side of Fig. 7e. This is consistent with what we observed in the cluster size distribution: TNFβ-TNFR2 signaling complexes prefer forming oligomers with larger maximal size and wider standard deviation.

3. Concluding discussions

The cytokines TNFα and TNFβ are key regulators of immune system through their binding with cell surface receptors TNFR1 and TNFR2. While signaling activated by TNFR1 modulates inflammatory and pro-apoptotic responses, TNFR2 mainly contributes to immune regulation and tissue regeneration. A comparative study on the ligand-receptor interactions between these two systems thus can provide a mechanistic understanding to TNF-mediated signaling in immune responses and further bring insights to the development of novel protein therapeutics that selectively target TNF receptors [71]. Using a residue-based kinetic Monte-Carlo simulation algorithm, we first showed that the binding between TNFα and TNFR1 is stronger and faster than the binding between TNFβ and TNFR2. Based on theoretically analyzing the data from all-atom molecular dynamic simulations, we further estimated the impacts of membrane confinement on the *cis*-interactions between receptors. We found that the *cis*-interactions between receptors will be drastically strengthened after ligand binding. Moreover, this effect on TNFR1 is almost twice as much as on TNFR2. Through the incorporation of all the information into a domain-based diffusion–reaction model, oligomerization of ligand-receptor complexes was simulated on a subcellular level. Different from the oligomers formed by TNFα-TNFR1 complexes which were stabilized very fast, the oligomerization of TNFβ-TNFR2 complexes is much slower but dynamic. More surprisingly, we found that the largest TNFβ-TNFR2 oligomers can almost double the size of the largest TNFα-TNFR1 oligomers. As we know, the intracellular regions of TNFR1 and TNFR2 associate with different downstream signaling molecules. For instance, the activation of TNFR1 leads to the recruitment of TNF receptor 1 associated protein with death domain (TRADD) in the cytoplasm [84], whereas the activation of TNFR2 leads to the recruitment of TNF receptor associated factor 2 (TRAF2) [85]. The recruitment of these signaling molecules is closely regulated by the dynamics and spatial patterns of receptor oligomerization. As a result, the difference in oligomerization between TNFR1 and TNFR2 described above throws light on the spatial–temporal regulation of TNF-mediated signaling pathways.

On a general level, oligomerization has also been observed for many other receptors in TNFR superfamily. For an example, highly organized oligomers of death receptor 5 (DR5) were observed on cell surfaces after the binding of TNF-related apoptosis-inducing ligand (TRAIL) [86]. In another case, experiments found that the formation of supramolecular clusters can be induced by the interactions between the extracellular domains of receptor Fas and its ligand FasL [87,88]. In principle, our multiscale modeling method can be naturally extended to compare the similarity and difference of oligomerization in these systems other than TNFR1 and TNFR2. Additionally, previous experimental measurements [79] and our comparative study [89] shows that the complexes formed between most receptors in the TNFR superfamily and their ligands are very similar on the structural level, but their binding constants span a wide range. Here, our simulation results further demonstrated that the difference in binding can lead into distinctive patterns of oligomerization. More specifically, we illustrated that the lower ratio of conformational fluctuations between monomeric and ligand-bound receptors plays an important role in maintaining the higher level of dynamics during oligomerization, which is able to result in the formation of ligand-receptor clusters with larger sizes. Therefore, our study provides insights to understand the mechanism of ligand-induced oligomerization for receptors in the entire TNFR superfamily. Finally, this approach will also potentially be used to study the functions of spatial organization in many cell surface receptors other than TNFR superfamily.

One issue which could lead to questionable results is the initial configuration. At the beginning of our simulations, we assume that TNFR receptors are arranged randomly in a monomeric state when they start to form interactions with ligands on the cell surface. However, previous experimental data indicate that TNFR receptors can form preassembly on the cell surface via their PLAD regions prior to ligand binding. This receptor preassembly was not taken account into our original simulations. In order to address this problem, an alternative starting model was carried out in which no TNF ligands were included in the systems during the early stage of simulations, so that monomeric TNF receptors had the opportunity to preassemble before ligand binding. Detailed simulation results

from this alternative model are summarized in Fig. S3. As shown in the figure, the TNFR1 system is represented in black and the TNFR2 system is represented in red. In both systems, ligands were introduced only after 3.5×10^7ns. The numbers of *cis*-interactions formed between receptor monomers were plotted in Fig. S3a as function of simulation time. The figure indicates that monomeric *cis*-interactions increased before they exposed to ligands, suggesting the ligand-independent preassembly of TNFR receptors on cell surface. These monomeric *cis*-interactions decayed soon after the introduction of ligands. In the meanwhile, the numbers of *cis*-interactions between ligand-receptor complexes started to increase, as shown in Fig. S3f. This indicates that the ligand-bound receptors have competed over the monomeric receptors to form *cis*-interactions. Similar phenomena were then observed as before in terms of the differences between the TNFR1 and TNFR2 systems. Oligomers with larger sizes were more likely to form by TNFβ-TNFR2 complexes (Fig. S3b and Fig. S3c), although less *trans*-interactions were attained in the system (Fig. S3e). All curves and distributions in the figure were derived by the average from 10 independent simulation trajectories.

Two representative snapshots were selected from one of these simulation trajectories. Fig. S5a shows the configuration of the TNFR1 system right before the ligand exposure, while final configuration of the trajectory is shown in Fig. S5b. Fig. S5a indicates that receptors were dimerized before ligand exposure through their *cis*-binding interfaces. The dimerization of TNFR1 prior to ligand binding has been recently observed in experiments using fluorescence resonance energy transfer (FRET) [90,91]. Fig. S5b further suggests that the introduction of TNF ligands induced higher-order oligomerization due to a multivalent effect. In detail, oligomerization of ligand-receptor complexes was achieved by the combination of *trans*- and *cis*-interactions, given the fact that the binding interfaces of these two interactions do not overlap in the extracellular region of TNFR. While *cis*-interactions link two receptors together, *trans*-interactions further link these dimerized receptors to trimeric TNF ligands which can simultaneously bind to three receptors. As a result, this spatial organization between dimeric receptors and trimeric ligands can lead into the formation of a hexagonal lattice on two-dimensional cell surface [20]. We further tested this model with simulations under a higher concentration and the results are illustrated in Fig. S4. Consistent results were obtained. Altogether, our tests confirmed that ligand-receptor complexes can still form oligomers when receptors are preassembled before ligand binding. Moreover, under this condition, the TNFR2 system still has the higher probability to form large oligomers than the TNFR1 system.

One limitation in this study is the calculation of configurational volume in Eqs. (1) and (2), in which the ranges of the Euler angles and height distributions are simply taken as twice the standard deviation. This simplification is based on the assumption that the conformational fluctuations of receptors and complexes follow normal distributions. In reality, however, the MD simulation results show that some of these distributions are not exactly Gaussian-like, especially the distributions for the Euler angles φ and ψ in TNFR1 and TNFR2 monomers (Fig. 5c and e). Although we believe that the wideness of conformational distributions can still be approximately captured by our simplified calculation, a thorough estimation of configurational volumes could be carried out by more rigorous method such as thermodynamic integration. Ideally, each potential microstate in the integral of these configurational volumes (Eq. S4 in the Supporting Information) should also be weighted with a Boltzmann distribution. There are also some other factors which are not taken account into current model. For instance, diffusions of TNFR receptors on the plasma membrane are much slower than soluble TNF ligands in the extracellular region, given the friction exerted by the lipid bilayer on their transmembrane domains. This effect is captured in our domain-based simulation by using different diffusion constants for TNF and TNFR. However, it is not included in equation (1), when the impact of membrane confinement on the association rates of *cis*-interaction between receptors was estimated. Fortunately, we expect that the effect of plasma membrane on diffusions of TNFR1 is very close to the effect on TNFR2, considering that both receptors are single-pass transmembrane proteins [62]. Finally, in current model, the system only contains TNF ligands and TNFR receptors. In reality, however, more than 20% of the cytoplasmic volume in a living cell is occupied by biomolecules [92]. Similarly, the plasma membranes of cells are crowded by various receptors and channels. Under these conditions, the kinetics of ligand-receptor binding is significantly affected [93,94]. This effect is neglected in current study, but can be considered in the future as follows. Specifically, in our domain-based simulation, many other proteins can be placed on the cell surface or in the extracellular region besides the interacting TNF ligands and receptors. Receptors and ligands will form repulsive collisions with these background molecules. The effect of crowding on both diffusion and association can therefore be studied.

4. Materials and methods

4.1. Domain-based diffusion–reaction simulation for ligand-receptor oligomerization

As described in our previous study, a simplified model is designed to simulate the dynamics of TNF ligand-receptor oligomerization on cell surface [72]. In brief, each subunit in a trimeric TNF ligand and each extracellular domain in a TNFR receptor is represented by a spherical rigid body which size is comparable to the corresponding protein structure. Cell plasma membrane is further represented by a flat surface at the bottom of a 3D simulation box, and the space above represents the extracellular region. Binding sites for the *trans*-interaction are assigned to each ligand subunit, as well as on the surface of the second domain in each receptor. Additionally, binding sites for the *cis*-interactions between receptors are assigned on the opposite side of their *trans*-binding sites. Given the initial configuration in which receptors are randomly distributed on plasma membrane and ligands are randomly distributed in the extracellular region, the dynamics of the system is evolved by following a diffusion–reaction algorithm. Within each simulation time step, ligands and receptors are selected by random order for stochastic diffusion as the first scenario. TNF ligands are free to move throughout the simulation box, while the movements of TNFR receptors are confined within plasma membrane. The probability and amplitude of these translational and rotational movements are determined by their corresponding diffusion coefficients. Moreover, periodic boundary condition is applied to move the molecules along x and y directions. As for the movements along z direction, if ligands move beyond the top of the simulation box, they will be bounced back. They are also not allowed to move below the plasma membrane. After the translational and rotational diffusions, the configuration of the system is updated. The new configuration will be accepted if there is no clash between any pair of proteins, otherwise the movements will be rejected.

The binding kinetics of ligand-receptor *trans*-interactions and receptor-receptor *cis*-interactions are followed after the new configuration is generated by the diffusion scenario. The distances between the binding sites of each protein are changed in the new configuration. These newly calculated distances are used to determine whether association can occur between a ligand and a receptor, or two receptors. Specifically, within each simulation

time step after diffusions, association between a TNF ligand and a TNFR receptor is triggered if the distance between the *trans*-binding sites of two molecules is below a predetermined cutoff value. The probability to form a *trans*-interaction is further determined by its association rate. Relatively, the probability to break a complex between a TNF ligand and a TNFR receptor is regulated by the dissociation rate of *trans*-interaction, which can be further calculated from its association rate and binding affinity. Similarly, association between two TNFR receptors is triggered if the distance between their *cis*-binding sites is below the same predetermined cutoff. The probability to form a *cis*-interaction is further determined by its association rate. Relatively, the probability to break a complex between two TNFR receptors is regulated by the *cis* dissociation rate, which can be further calculated from the *cis* association rate and binding affinity. If a TNF ligand binds to a receptor, or two receptors form a lateral dimer, the entire complex will move as a single unit on plasma membrane. When more ligands and receptors join through their *trans* or *cis* interactions, the size of the oligomer will continue growing and its diffusions become slower. An oligomer will stop diffusing if it contains more than two full-size signaling complexes. This assumption is based on the following evidences. It was found in previous single molecule imaging experiment that upon oligomerization, diffusions were reduced by at least an order of magnitude for membrane proteins on the same cell surface [95]. Furthermore, as the size of oligomers grew, diffusions became even slower. It was speculated that these oligomers formed through *cis*-interactions between receptors were trapped due to the enhancement of connections between their intracellular domains and cytoskeleton. Given this information, in order to avoid further computational complexity, oligomers consisting of more than two ligand-receptor complexes are set as static in our simulation, even though their mobility was still detectable in the experiment. We believe that our simulation outputs will not be significantly affected by this simplification.

As above diffusion–reaction process iterates in both Cartesian and compositional spaces, the spatial patterns in the system will evolve and finally reach equilibrium. Finally, in order to evaluate the dependence of modeled systems on different factors, sensitivity analysis was applied to the simulations under different concentrations and various binding rates of ligand-receptor interactions. Detailed results from the analysis are summarized in Fig. S1 for lower concentration and Fig. S2 for higher concentration.

4.2. Residue-based kinetic Monte-Carlo simulation for protein–protein association

We applied a previously developed kinetic Monte-Carlo simulation algorithm [76] to estimate the association between TNF ligands and TNFR receptors, as well as the association between two TNFR receptors. A coarse-grained model is used in the simulation to represent protein structures. Each residue in a protein is simplified by two beads: its Cα atom and a representative center of its side-chain which was selected based on the chemical properties of each specific type of amino acid. At the beginning of simulation, the coarse-grained models of two proteins are separated and placed randomly in the 3D simulation space as an initial conformation whereas their corresponding binding interfaces are within the range of a given distance cutoff d_c. Following this initial set-up, random diffusions are carried out for each protein along its three translational and rotational degrees of freedom. A physics-based scoring function that contains electrostatic interaction and hydrophobic effect is used to estimate the binding energy between two proteins and guide their diffusions of proteins. The probability whether diffusional movements can be accepted or not is based on the Metropolis criterion in which the binding energies before and after the diffusions are compared. At the end of each simulation step, the newly formed configuration of the protein complex will be further inspected. The simulation will be terminated if an encounter complex is successfully formed between two proteins through their corresponding interface, through predefined association criteria. Otherwise, above simulation procedure will be repeatedly iterated until the trajectory reaches the maximal time duration.

In order to practically estimate the effective association rate, above simulation algorithm is performed under different distance cutoffs in parallel, while a large number of trajectories are generated under each specific value of distance cutoff. All these trajectories start from different initial conformations in which two proteins are placed with different positions and relative orientations, but the initial distances between their binding interfaces are all below the same cutoff value. Proteins fail to form a complex and diffuse away within some trajectories, while native-like encounter complexes can be successfully formed at the end of other trajectories. By counting how many encounter complexes were successfully formed among all trajectories, the probability of association can be calculated for a given distance cutoff. As shown in Fig. 3b and d, the association probabilities for both *trans*- and *cis*-interactions drop when the values of distance cutoff increase. Based on the distribution of these calculated probabilities, the values of association rates for these interactions can be derived as follows. According to our previous study [96], an effective distance of association is assigned where the association probability falls below 30% of its highest value. The effective association probability is further defined as the average value of all probabilities which distance cutoffs are below the effective distance. The association rate is thereby the effective association probability divided by the simulation time step. Using the *trans*-interaction between TNFα and TNFR1 (black curve in Fig. 3b) as an example, its highest value of association probability is 0.33. This gives the effective distance of association equals 17 Å and the effective association probability equals 0.25. As a result, we obtain the association rate of 0.025 ns^{-1} for a simulation time step of 10 ns.

In order to link the residue-based and the domain-based simulations within the same time-scale, the maximal time duration to terminate each residue-based simulation trajectory was set to be equal to the length of each time step in the domain-based simulation, so that the association rates calculated from the residue-based method can be effectively used in the domain-based model. In detail, each trajectory of residue-based simulation contains maximally 10^3 steps and the length of each step is 0.01 ns. As a result, the maximal length of each residue-based simulation trajectory is 10 ns, which is the time step adopted in the domain-based simulation [96]. Here it is also worth pointing out that the association rates calculated from the residue-based simulations have a different definition from the on rates which are experimentally measured by SPR or ITC. These rate constants are derived as input parameters for our domain-based diffusion–reaction simulations. They estimate the probability of association within each time step of domain-based simulations, if the distance of binding sites between a single pair of interacting proteins is below a predetermined cutoff value. Therefore, while the experimental on rates have the standard unit in $M^{-1}s^{-1}$, our association rates have the unit in ns^{-1}. This association rate can be converted to the standard on rate with the unit of $M^{-1}s^{-1}$ by the analysis used in our previous study [75]. Finally, although the rotational degrees of freedom have already been incorporated in the calculation of association rates, they only cover the situation after the binding sites of two interacting proteins are close enough to each other. On the other hand, the corresponding degrees of freedom for ligands and receptors separated farther than the distance cutoff are taken into account by the translational and rotational diffusions in the domain-based simulations.

4.3. All-atom molecular dynamic simulation for protein conformational fluctuations

In order to estimate the difference between 3D and 2D association rates of receptor *cis*-interactions due to the membrane confinement, all-atom molecular dynamics simulation was applied to study the conformational fluctuations of single TNFR receptors, as well as the entire signaling complexes in lipid bilayer. The model of a single receptor contains its extracellular domains, the transmembrane helix, and a linker region that connect these two segments, while the model of a signaling complex comprises a trimeric ligand and three bound receptors. The atomic coordinates of TNFR1′s extracellular domains were adopted from the crystal structure with PDB id 1EXT, while TNFR2′s extracellular domains were obtained from the crystal structure with PDB id 3ALQ. For TNFα-TNFR1 system, a structure of the complex became available very recently [20]. However, the trimeric ligand in this asymmetric complex is distorted. Therefore, it is not used in our study. The initial structure of TNFα-TNFR1 complex was adopted from the computational model that was previously built by Xie's group [77]. In contrast, no experimental structure is available for TNFβ-TNFR2 signaling complex. As a result, the initial conformation of ligand TNFβ in the complex was taken from the PDB id 1TNR. The relative orientations between TNFβ and TNFR2 were adopted from the crystal structure of TNFα-TNFR2 complex. Rigid-body superposition and alignment were applied using VMD to obtain the final model of TNFβ-TNFR2 complex. Transmembrane regions of receptors in all these systems were built as standard α-helices, and their linkers between transmembrane and extracellular regions were modeled by the online server, ModLoop [97]. The transmembrane domain of each receptor was further embedded in a lipid bilayer comprised of around 500 POPC molecules. Counter-ions (Na+, Cl-) were added to neutralize the net charge in the simulation box and to maintain an appropriate ionic strength (0.1 M).

After the construction of the initial models, all systems were equilibrated at 310 K and 1 atm to remove unrealistic contacts. After equilibration, simulations were carried out using GROMACS with the CHARMM36m force field and the TIP3P water. Covalent bonds were constrained using the LINCS algorithm, and an integration time step of 2 fs was used together with the leapfrog integrator. A cutoff of 13 Å was used for van der Waals interactions, and electrostatic interactions were calculated with the particle mesh technique for Ewald summations, also with a cutoff of 13 Å. Temperature and pressure are controlled using the v-rescale thermostat (τ_T = 0.1 ps) and the Parrinello-Rahman barostat (τ_P = 0.1 ps), respectively. An overview of the simulation systems in this study can be found in Table S1. A 400 ns trajectory was generated for TNR1. For TNR2, because the linker region between its extracellular and transmembrane domains is longer, two independent simulation trajectories were produced to enhance conformational sampling. The length of each trajectory is 300 ns. Different initial conformation of the linker region was adopted in each trajectory. For ligand-receptor complexes, a 500 ns trajectory was generated for both TNFα-TNFR1 and TNFβ-TNFR2 systems. In summary, the total all-atom MD simulation time for this study is 2 microseconds.

Based on the all-atom simulation results, we first calculated the backbone root mean square deviation (RMSD). The RMSD of the extracellular domain for TNFR1 and TNFR2 are plotted in Fig. S6a as a function of simulation time. The figure indicates that the RMSD of TNFR1 is lower than TNFR2. Similarly, the RMSD of TNFα-TNFR1 and TNFβ-TNFR2 complexes are compared in Fig. S6b as a function of simulation time. The figure indicates that the RMSD of TNFβ-TNFR2 is higher than TNFα-TNFR1 complex. In addition to RMSD, the root mean square fluctuations (RMSF) were also calculated for each residue. The RMSF of TNFR1 and TNFR2 are plotted in Fig. S7a along with the residue number in their extracellular domains, while the RMSF of TNFα-TNFR1 and TNFβ-TNFR2 complexes are plotted in Fig. S7b. The figures suggest that residue fluctuations in both monomeric and ligand-bound TNFR2 are higher than TNFR1. Moreover, the range of translational fluctuations along the z axis, Δh, in the single receptor and the signaling complex, as well as the rotational distributions of their three Euler angles, Δφ, Δθ, and Δψ were further calculated. Detailed analysis is described in the Results.

CRediT authorship contribution statement

Zhaoqian Su: Methodology, Validation, Formal analysis, Investigation, Data curation, Writing - original draft, Writing - review & editing, Visualization. **Kalyani Dhusia:** Validation, Formal analysis. **Yinghao Wu:** Methodology, Investigation, Resources, Supervision, Funding acquisition, Project administration, Writing - original draft, Writing - review & editing.

Declaration of Competing Interest

The authors declare that they have no known competing financial interests or personal relationships that could have appeared to influence the work reported in this paper.

Acknowledgements

This work was supported by the National Institutes of Health under Grant Numbers R01GM122804. The work is also partially supported by a start-up grant from Albert Einstein College of Medicine. Computational support was provided by Albert Einstein College of Medicine High Performance Computing Center.

Author contributions

Z.S. and Y.W. designed research; Z.S. and Y.W. performed research; Z.S., K. D. and Y.W. analyzed data; Z.S. and Y.W. wrote the paper.

Competing financial interests

The authors declare no competing financial interests.

Appendix A. Supplementary data

Supplementary data to this article can be found online at https://doi.org/10.1016/j.csbj.2021.03.024.

References

[1] Li S. Mechanisms of cellular signal transduction. Int J Biol Sci 2005;1(4):152.
[2] Packard B, Receptor phosphorylation and signal transduction across plasma-membranes. Trends Biochem Sci 1985, 10(4):138-138.
[3] Ullrich A, Schlessinger J. Signal transduction by receptors with tyrosine kinase-activity. Cell 1990;61(2):203–12.
[4] Krauss RS. Regulation of promyogenic signal transduction by cell-cell contact and adhesion. Exp Cell Res 2010;316(18):3042–9.
[5] Lalli E, Sassone-Corsi P. Signal-transduction and gene-regulation - the nuclear response to cAMP. J Biol Chem 1994;269(26):17359–62.
[6] Cuatrecasas P. Membrane receptors. Annu Rev Biochem 1974;43(1):169–214.
[7] Locksley RM, Killeen N, Lenardo MJ. The TNF and TNF receptor superfamilies: integrating mammalian biology. Cell 2001;104(4):487–501.
[8] MacEwan DJ. TNF ligands and receptors–a matter of life and death. Br J Pharmacol 2002;135(4):855–75.
[9] Sedger LM, McDermott MF. TNF and TNF-receptors: From mediators of cell death and inflammation to therapeutic giants - past, present and future. Cytokine Growth Factor Rev 2014;25(4):453–72.
[10] Ghosh S, Baltimore D. Activation in vitro of NF-kappa B by phosphorylation of its inhibitor I kappa B. Nature 1990;344(6267):678–82.

[11] Sen R, Baltimore D. Inducibility of kappa immunoglobulin enhancer-binding protein Nf-kappa B by a posttranslational mechanism. Cell 1986;47(6):921–8.
[12] Gilmore TD. Introduction to NF-kappaB: players, pathways, perspectives. Oncogene 2006;25(51):6680–4.
[13] Brasier AR. The NF-kappaB regulatory network. Cardiovasc Toxicol 2006;6 (2):111–30.
[14] Bell G. Models for the specific adhesion of cells to cells. Science (New York, NY) 1978;200(4342):618–27.
[15] Bell GI, Dembo M, Bongrand P. Cell adhesion. Competition between nonspecific repulsion and specific bonding. Biophys J 1984;45(6):1051–64.
[16] Cairo CW. Signaling by committee: Receptor clusters determine pathways of cellular activation. ACS Chem Biol 2007;2(10):652–5.
[17] Hartman NC, Groves JT. Signaling clusters in the cell membrane. Curr Opin Cell Biol 2011;23(4):370–6.
[18] Vanamee ÉS, Faustman DL. Structural principles of tumor necrosis factor superfamily signaling. Sci Signaling 2018;11(511).
[19] Karathanasis C, Medler J, Fricke F, Smith S, Malkusch S, Widera D, et al. Single-molecule imaging reveals the oligomeric state of functional TNFα-induced plasma membrane TNFR1 clusters in cells. Sci Signaling 2020;13(614).
[20] McMillan D, Martinez-Fleites C, Porter J, Fox D, Davis R, Mori P, et al. Structural insights into the disruption of TNF-TNFR1 signalling by small molecules stabilising a distorted TNF. Nat Commun 2021;12(1).
[21] Cebecauer M, Spitaler M, Serge A, Magee AI. Signalling complexes and clusters: functional advantages and methodological hurdles. J Cell Sci 2010;123 (3):309–20.
[22] Shi D, Lv X, Zhang Z, Yang X, Zhou Z, Zhang L, et al. Smoothened oligomerization/higher order clustering in lipid rafts is essential for high Hedgehog activity transduction. J Biol Chem 2013;288(18):12605–14.
[23] Yi JC, Samelson LE. Microvilli set the stage for T-cell activation. Proc Natl Acad Sci USA 2016;113(40):11061–2.
[24] Aricescu AR, Jones EY. Immunoglobulin superfamily cell adhesion molecules: zippers and signals. Curr Opin Cell Biol 2007;19(5):543–50.
[25] Wang W, Yang Y, Wang S, Nagaraj VJ, Liu Q, Wu J, et al. Label-free measuring and mapping of binding kinetics of membrane proteins in single living cells. Nat Chem 2012;4(10):846–53.
[26] Li G, Xi N, Wang DH. Probing membrane proteins using atomic force microscopy. J Cell Biochem 2006;97(6):1191–7.
[27] Müller DJ, Engel A. Atomic force microscopy and spectroscopy of native membrane proteins. Nat Protoc 2007;2(9):2191–7.
[28] Groves JT, Parthasarathy R, Forstner MB. Fluorescence imaging of membrane dynamics. Annu Rev Biomed Eng 2008;10(1):311–38.
[29] Schwarzenbacher M, Kaltenbrunner M, Brameshuber M, Hesch C, Paster W, Weghuber J, et al. Micropatterning for quantitative analysis of protein-protein interactions in living cells. Nat Methods 2008;5(12):1053–60.
[30] Johnson AE. Fluorescence approaches for determining protein conformations, interactions and mechanisms at membranes. Traffic 2005;6(12):1078–92.
[31] Wallrabe H, Periasamy A. Imaging protein molecules using FRET and FLIM microscopy. Curr Opin Biotechnol 2005;16(1):19–27.
[32] Axelrod D. Total internal reflection fluorescence microscopy in cell biology. Traffic 2001;2(11):764–74.
[33] Pierce MM, Raman CS, Nall BT. Isothermal titration calorimetry of protein-protein interactions. Methods 1999;19(2):213–21.
[34] Daghestani HN, Day BW. Theory and applications of surface plasmon resonance, resonant mirror, resonant waveguide grating, and dual polarization interferometry biosensors. Sensors 2010;10(11):9630–46.
[35] Dustin ML, Bromley SK, Davis MM, Zhu C. Identification of self through two-dimensional chemistry and synapses. Annu Rev Cell Dev Biol 2001;17 (1):133–57.
[36] Dustin ML, Ferguson LM, Chan PY, Springer TA, Golan DE. Visualization of CD2 interaction with LFA-3 and determination of the two-dimensional dissociation constant for adhesion receptors in a contact area. J Cell Biol 1996;132 (3):465–74.
[37] Hollingsworth SA, Dror RO. Molecular dynamics simulation for all. Neuron 2018;99(6):1129–43.
[38] Karplus M, Petsko GA. Molecular dynamics simulations in biology. Nature 1990;347(6294):631–9.
[39] Perilla JR, Goh BC, Cassidy CK, Liu Bo, Bernardi RC, Rudack T, et al. Molecular dynamics simulations of large macromolecular complexes. Curr Opin Struct Biol 2015;31:64–74.
[40] Ando T, Skolnick J. Crowding and hydrodynamic interactions likely dominate in vivo macromolecular motion. Proc Natl Acad Sci USA 2010;107 (43):18457–62.
[41] Skolnick J, Ando T, Simulation of protein diffusion and folding in a Protocell. Abstracts Pap Am Chem Soc 2009, 238:717-717.
[42] McGuffee SR, Elcock AH. Diffusion, crowding & protein stability in a dynamic molecular model of the bacterial cytoplasm. PLoS Comput Biol 2010;6(3).
[43] Slepchenko BM, Schaff JC, Carson JH, Loew LM. Computational cell biology: spatiotemporal simulation of cellular events. Annu Rev Biophys Biomol Struct 2002;31(1):423–41.
[44] Slepchenko BM, Schaff JC, Macara I, Loew LM. Quantitative cell biology with the virtual cell. Trends Cell Biol 2003;13(11):570–6.
[45] Francke C, Postma PW, Westerhoff HV, Blom JG, Peletier MA. Why the phosphotransferase system of Escherichia coli escapes diffusion limitation. Biophys J 2003;85(1):612–22.
[46] Hattne J, Fange D, Elf J. Stochastic reaction-diffusion simulation with MesoRD. Bioinformatics (Oxford, England) 2005;21(12):2923–4.
[47] Ander M, Beltrao P, Di Ventura B, Ferkinghoff-Borg J, Foglierini M, Kaplan A, et al., SmartCell, a framework to simulate cellular processes that combines stochastic approximation with diffusion and localisation: analysis of simple networks. Syst Biol (Stevenage) 2004, 1(1):129-138.
[48] Rodriguez JV, Kaandorp JA, Dobrzynski M, Blom JG, Spatial stochastic modelling of the phosphoenolpyruvate-dependent phosphotransferase (PTS) pathway in Escherichia coli. Bioinformatics (Oxford, England) 2006, 22 (15):1895-1901.
[49] Stiles Jr, Bartol TM. Monte Carlo methods for simulating realistic synaptic microphysiology using MCell. Computational Neuroscience 2001:87–127.
[50] Andrews SS, Bray D. Stochastic simulation of chemical reactions with spatial resolution and single molecule detail. Phys Biol 2004;1(3):137–51.
[51] Ridgway D, Broderick G, Lopez-Campistrous A, Ru'aini M, Winter P, Hamilton M, et al. Coarse-grained molecular simulation of diffusion and reaction kinetics in a crowded virtual cytoplasm. Biophys J 2008;94(10):3748–59.
[52] Frazier Z, Alber F. A computational approach to increase time scales in brownian dynamics-based reaction-diffusion modeling. J Comput Biol 2012;19 (6):606–18.
[53] Ayton GS, Noid WG, Voth GA. Multiscale modeling of biomolecular systems: in serial and in parallel. Curr Opin Struct Biol 2007;17(2):192–8.
[54] Noid WG, Chu J-W, Ayton GS, Krishna V, Izvekov S, Voth GA, et al. The multiscale coarse-graining method. I. A rigorous bridge between atomistic and coarse-grained models. J Chem Phys 2008;128(24):244114.
[55] Ayton GS, Voth GA. Systematic multiscale simulation of membrane protein systems. Curr Opin Struct Biol 2009;19(2):138–44.
[56] Hirakis S, Boras B, Votapka L, Malmstrom R, McCulloch A, Amaro R. Bridging scales through multiscale modeling: a case study on protein kinase A. Front Physiol 2015;6(250).
[57] Gilabert JF, Gracia Carmona O, Hogner A, Guallar V. Combining Monte Carlo and molecular dynamics simulations for enhanced binding free energy estimation through Markov state models. J Chem Inf Model 2020;60 (11):5529–39.
[58] de Jong DH, Singh G, Bennett WFD, Arnarez C, Wassenaar TA, Schäfer LV, et al. Improved parameters for the martini coarse-grained protein force field. J Chem Theory Comput 2013;9(1):687–97.
[59] Ekimoto T, Ikeguchi M. Multiscale molecular dynamics simulations of rotary motor proteins. Biophys Rev 2018;10(2):605–15.
[60] Saunders MG, Voth GA. Coarse-graining methods for computational biology. Annu Rev Biophys 2013;42(1):73–93.
[61] Ansell TB, Song W, Sansom MSP. The glycosphingolipid GM3 modulates conformational dynamics of the glucagon receptor. Biophys J 2020;119 (2):300–13.
[62] Wajant H, Siegmund D. TNFR1 and TNFR2 in the control of the life and death balance of macrophages. Front Cell Dev Biol 2019;7:91.
[63] Tartaglia LA, Ayres TM, Wong GHW, Goeddel DV. A novel domain within the 55 kd TNF receptor signals cell death. Cell 1993;74(5):845–53.
[64] Xie P. TRAF molecules in cell signaling and in human diseases. J Mol Signaling 2013;8(1):7.
[65] Eck MJ, Sprang SR. The structure of tumor necrosis factor-alpha at 2.6 A resolution. Implications for receptor binding. J Biol Chem 1989;264 (29):17595–605.
[66] Idriss HT, Naismith JH. TNF alpha and the TNF receptor superfamily: structure-function relationship(s). Microsc Res Technol 2000;50(3):184–95.
[67] Banner DW, D'Arcy A, Janes W, Gentz R, Schoenfeld HJ, Broger C, et al. Crystal structure of the soluble human 55 kd TNF receptor-human TNF beta complex: implications for TNF receptor activation. Cell 1993;73(3):431–45.
[68] Mukai Y, Nakamura T, Yoshikawa M, Yoshioka Y, Tsunoda S, Nakagawa S, et al. Solution of the structure of the TNF-TNFR2 complex. Sci Signal 2010, 3(148): ra83.
[69] Naismith JH, Devine TQ, Brandhuber BJ, Sprang SR. Crystallographic evidence for dimerization of unliganded tumor necrosis factor receptor. J Biol Chem 1995;270(22):13303–7.
[70] Wajant H, Pfizenmaier K, Scheurich P. Tumor necrosis factor signaling. Cell Death Differ 2003;10(1):45–65.
[71] Fischer R, Kontermann RE, Pfizenmaier K. Selective targeting of TNF receptors as a novel therapeutic approach. Front Cell Dev Biol 2020;8:401.
[72] Su Z, Wu Y. A computational model for understanding the oligomerization mechanisms of TNF receptor superfamily. Comput Struct Biotechnol J 2020;18:258–70.
[73] Chan F-M. Three is better than one: pre-ligand receptor assembly in the regulation of TNF receptor signaling. Cytokine 2007;37(2):101–7.
[74] Chan FK, Chun HJ, Zheng L, Siegel RM, Bui KL, Lenardo MJ. A domain in TNF receptors that mediates ligand-independent receptor assembly and signaling. Science (New York, NY) 2000;288(5475):2351–4.
[75] Xie Z-R, Chen J, Wu Y. A coarse-grained model for the simulations of biomolecular interactions in cellular environments. J Chem Phys 2014;140 (5):054112. https://doi.org/10.1063/1.4863992.
[76] Xie ZR, Chen J, Wu Y. Predicting protein-protein association rates using coarse-grained simulation and machine learning. Sci Rep 2017;7:46622.
[77] Chen S, Feng Z, Wang Y, Ma S, Hu Z, Yang P, et al. Discovery of novel ligands for TNF-alpha and TNF receptor-1 through structure-based virtual screening and biological assay. J Chem Inf Model 2017;57(5):1101–11.
[78] Wu Y, Vendome J, Shapiro L, Ben-Shaul A, Honig B. Transforming binding affinities from three dimensions to two with application to cadherin clustering. Nature 2011;475(7357):510–3.

[79] Lang I, Füllsack S, Wyzgol A, Fick A, Trebing J, Arana JAC, et al. Binding studies of TNF receptor superfamily (TNFRSF) receptors on intact cells. J Biol Chem 2016;291(10):5022–37.
[80] Zhang C, Liu S, Zhou H, Zhou Y. An accurate, residue-level, pair potential of mean force for folding and binding based on the distance-scaled, ideal-gas reference state. Protein Sci 2004;13(2):400–11.
[81] Brameshuber M, Kellner F, Rossboth BK, Ta H, Alge K, Sevcsik E, et al. Monomeric TCRs drive T cell antigen recognition. Nat Immunol 2018;19 (5):487–96.
[82] Aragon S, Hahn DK. Precise boundary element computation of protein transport properties: Diffusion tensors, specific volume, and hydration. Biophys J 2006;91(5):1591–603.
[83] Xie ZR, Chen J, Wu Y, Linking 3D and 2D binding kinetics of membrane proteins by multi-scale simulations. Protein Sci 2014.
[84] Park YC, Ye H, Hsia C, Segal D, Rich RL, Liou HC, et al. A novel mechanism of TRAF signaling revealed by structural and functional analyses of the TRADD-TRAF2 interaction. Cell 2000, 101(7):777-787.
[85] Zheng C, Kabaleeswaran V, Wang Y, Cheng G, Wu H. Crystal structures of the TRAF2: cIAP2 and the TRAF1: TRAF2: cIAP2 complexes: affinity, specificity, and regulation. Mol Cell 2010;38(1):101–13.
[86] Naval J, de Miguel D, Gallego-Lleyda A, Anel A, Martinez-Lostao L. Importance of TRAIL molecular anatomy in receptor oligomerization and signaling. implications for cancer therapy. Cancers (Basel) 2019;11(4).
[87] Siegel RM, Muppidi JR, Sarker M, Lobito A, Jen M, Martin D, et al. SPOTS: signaling protein oligomeric transduction structures are early mediators of death receptor-induced apoptosis at the plasma membrane. J Cell Biol 2004, 167(4):735-744.
[88] Henkler F, Behrle E, Dennehy KM, Wicovsky A, Peters N, Warnke C, et al. The extracellular domains of FasL and Fas are sufficient for the formation of supramolecular FasL-Fas clusters of high stability. J Cell Biol 2005, 168 (7):1087-1098.
[89] Su Z, Wu Y: A systematic test of receptor binding kinetics for ligands in tumor necrosis factor superfamily by computational simulations. Int J Mol Sci 2020, 21(5).
[90] Lo CH, Huber EC, Sachs JN, Conformational states of TNFR1 as a molecular switch for receptor function. Protein Sci 2020, 29(6):1401-1415.
[91] Lo CH, Schaaf TM, Grant BD, Lim CK, Bawaskar P, Aldrich CC, et al. Noncompetitive inhibitors of TNFR1 probe conformational activation states. Sci Signal 2019, 12(592).
[92] Feig M, Yu I, Wang P-H, Nawrocki G, Sugita Y. Crowding in cellular environments at an atomistic level from computer simulations. J Phys Chem B 2017;121(34):8009–25.
[93] Kozer N, Schreiber G. Effect of crowding on protein - Protein association rates: fundamental differences between low and high mass crowding agents. J Mol Biol 2004;336(3):763–74.
[94] Minton AP. The influence of macromolecular crowding and macromolecular confinement on biochemical reactions in physiological media. J Biol Chem 2001;276(14):10577–80.
[95] Iino R, Koyama I, Kusumi A. Single molecule imaging of green fluorescent proteins in living cells: E-cadherin forms oligomers on the free cell surface. Biophys J 2001;80(6):2667–77.
[96] Wang B, Xie ZR, Chen J, Wu Y, Integrating structural information to study the dynamics of protein-protein interactions in cells. Structure (London, England: 1993) 2018, 26(10):1414-1424.e1413.
[97] Fiser A, Sali A. ModLoop: automated modeling of loops in protein structures. Bioinformatics (Oxford, England) 2003;19(18):2500–1.